Material: Ferritic Steel: F82H
Property: ΔDBTT vs. Helium Concentration
Data: Experimental

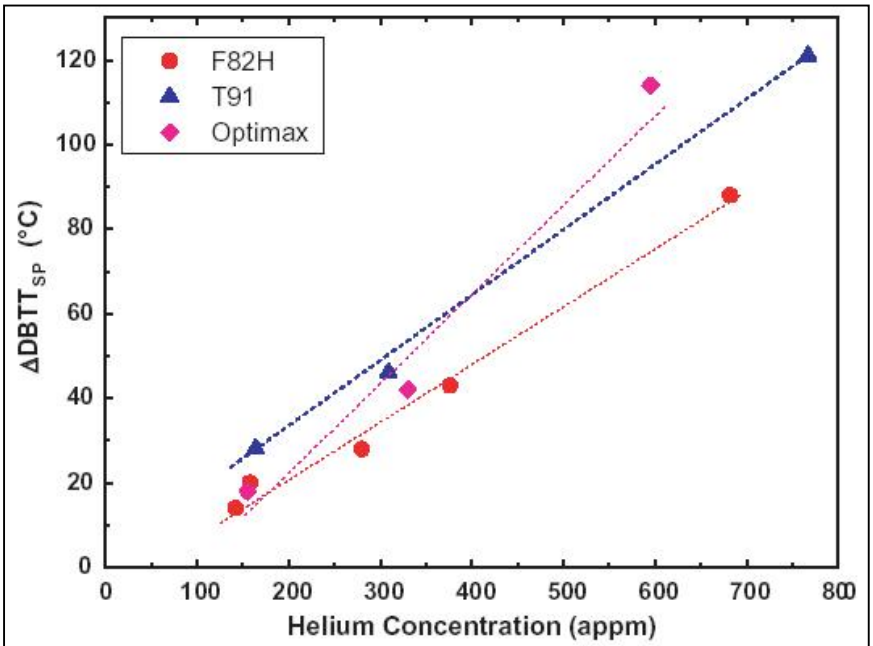

Fig. 11. The $DBTT_{SP}$ as a function of helium concentration

Source:
Journal of Nuclear Materials 323 2-3 (2003) 360-367

Title of paper (or report) this figure appeared in:
Small Punch Tests on Martensitic/Ferritic Steels F82H, T91, and Optimax-A Irradiated in SINQ Target-3

Author of paper or graph:
X. Jia, Y. Dai

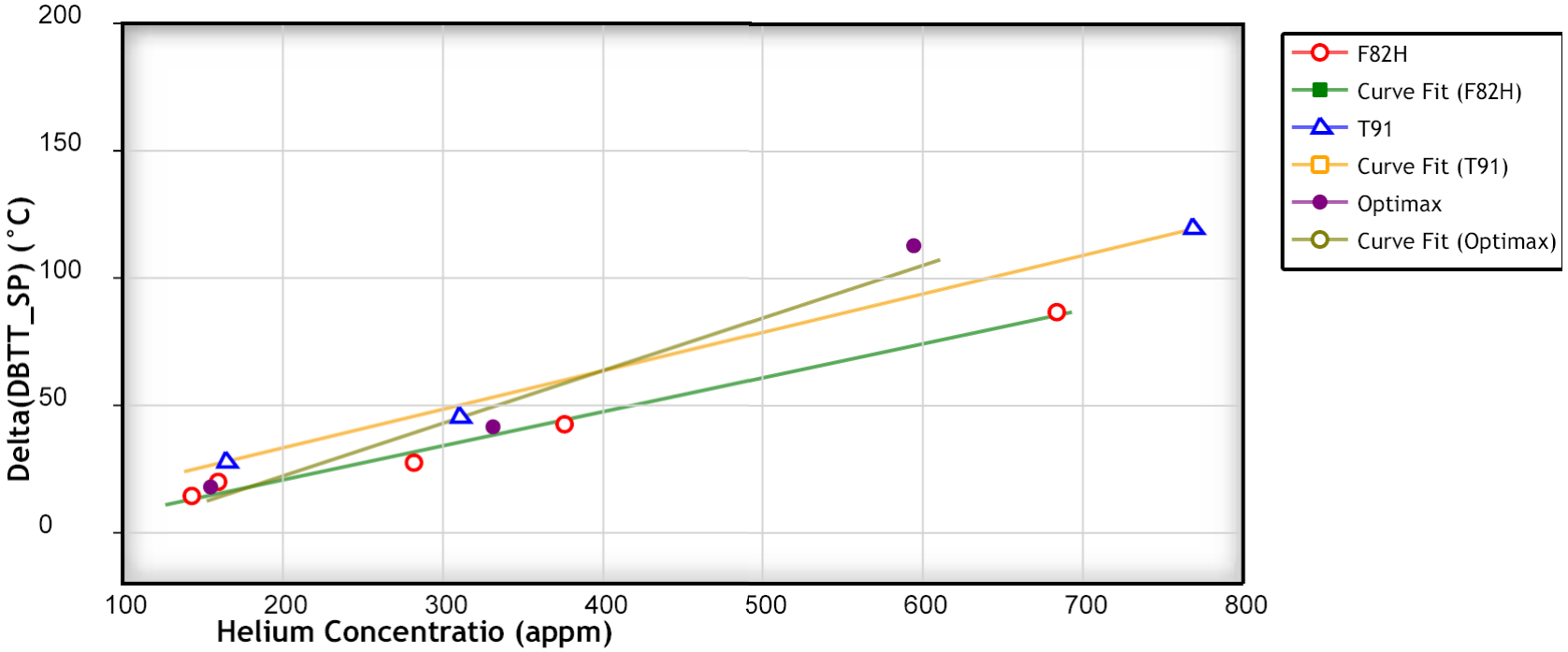

The DBTT_SP as a function of helium concentration.

Reference:

Author: *X. Jia, Y. Dai*

Title: *Small Punch Tests on Martensitic/Ferritic Steels F82H, T91, and Optimax-A Irradiated in SINQ Target-3*

Source: *Journal of Nuclear Materials, 2003, Volume 323, Number 2-3, Page 360-367*, [PDF]

View Data

Author Comments

Plot Format:

Y-Scale: ◉ linear ○ log ○ ln

X-Scale: ◉ linear ○ log ○ ln

Update Close Window

Available online at www.sciencedirect.com
SCIENCE DIRECT®
Journal of Nuclear Materials 323 (2003) 360–367
journal of nuclear materials
www.elsevier.com/locate/jnucmat

Small punch tests on martensitic/ferritic steels F82H, T91 and Optimax-A irradiated in SINQ Target-3

X. Jia, Y. Dai *

Spallation Neutron Source Division, Paul Scherrer Institut, 5232 Villigen PSI, Switzerland

Abstract

Small punch (SP) tests were conducted in a temperature range from −190 to 80 °C on martensitic/ferritic steels F82H, T91 and Optimax-A irradiated in SINQ Target-3 up to 9.4 dpa in a irradiation temperature range of 90–275 °C. Results demonstrate: (a) the irradiation hardening deduced from SP tests is reasonably consistent with the results obtained by tensile tests; (b) with increasing irradiation dose, the SP yield load increases at all test temperatures, while the displacement at the maximum load and the total displacement at failure decrease; (c) the ductile-to-brittle transition temperature ($DBTT_{SP}$) increases with increasing irradiation dose, and does so more quickly at irradiation doses above ~6–7 dpa; in addition, the $\Delta DBTT_{SP}$ increases linearly with helium content.

PACS: 61.80.−x; 61.82.Bg; 62.20.Mk

1. Introduction

The micro-structural and metallurgical changes from high-energy proton and neutron irradiation cause a significant degradation of the mechanical properties of materials. A major concern for martensitic/ferritic steels such as F82H and T91 is the irradiation-induced embrittlement [1,2]. These steels are considered as candidate materials for the first wall of fusion reactors and the containers of the liquid target of spallation neutron sources and accelerator driven systems (ADS) in the future.

Due to the limited space available for irradiation experiments in nuclear reactors and charged particle irradiation facilities. SP testing, which uses 3 mm diameter TEM disks to evaluate mechanical properties, is now considered as a promising method of evaluating fracture behaviour in the ductile-to-brittle transition temperature (DBTT) range [3–5]. In the present work, the embrittlement of F82H, T91 and Optimax-A steels irradiated in a proton and neutron mixed spectrum has been examined by using the small punch technique.

2. Experimental

T91 steel received from Oak Ridge national laboratory has a composition in wt% of 8.32 Cr, 0.86 Mo, 0.48 Mn, 0.20 V, 0.06 Ni, 0.06 Nb and 0.09 C with the balance Fe. The plate (Heat #30176) was cold-rolled from 6 to 3 mm, and was subjected to the following heat treatment: normalized at 1040 °C for 1 h, air cooled then tempered at 760 °C for 1 h [6]. F82H steel (IEA Heat 9741) used in this irradiation has a composition in wt% of 7.65 Cr, 2 W, 0.16 Mn, 0.16 V, 0.02 Ta, 0.11 Si and 0.09 C with the balance Fe. The 15 mm thick plate was subjected to the following heat treatment: normalized at 1040 °C for 38 min, air cooled then tempered at 750 °C for 1 h, to produce a final fully martensite lath structure [7]. Optimax-A steel used in this study has a composition in wt% of 9.3 Cr, 0.09 Mo, 0.60 Mn, 0.24 V, 0.97 W, 0.02 Si and 0.098 C with the balance Fe. The 8 mm plate was subjected to a heat treatment: normalized at 1050 °C for 1 h, air cooled then tempered at 750 °C for 2 h [8].

* Corresponding author. Tel.: +41-56 310 4171; fax: +41-56 310 4529.
E-mail address: yong.dai@psi.ch (Y. Dai).

0022-3115/$ - see front matter © 2003 Elsevier B.V. All rights reserved.
doi:10.1016/j.jnucmat.2003.08.018

Table 1
Irradiation conditions and SP test results of F82H, T91 and Optimax-A SP samples

Materials	Specimen ID.	dpa	Irrd. temp. (°C)	He (appm)	$DBTT_{SP}$ (°C)	$\Delta DBTT_{SP}$ (°C)	USE (J)
F82H	Un-irr	–	–	–	−164	–	0.22
	Pa	2.5	80 ± 8	140	−150	14	0.21
	Pb	4.5	150 ± 10	285	−143	21	0.20
	Pc	3.5	98 ± 8	160	−136	28	0.19
	Pd	6.5	180 ± 15	375	−121	43	0.18
	Pe	8.6	265 ± 20	680	−76	88	0.17
T91	Un-irr	–	–	–	−153	–	0.17
	Ia	2.8	90 ± 8	165	−125	28	0.16
	Ib	4.8	160 ± 15	310	−110	43	0.15
	Ie	9.4	275 ± 20	770	−35	118	0.13
Optimax-A	Un-irr	–	–	–	−165	–	0.19
	Na	4.4	130 ± 10	260	−148	17	0.17
	Nb	6.1	170 ± 15	330	−123	42	0.16
	Nc	8.2	240 ± 20	595	−50	115	0.14

In the first SINQ target irradiation program (STIP-I), specimens of different kinds of materials and various sizes were put into 10 rods for irradiation [9]. The positions of all these special rods were in the central columns of the target. SP samples of F82H, T91 and Optimax-A steels were put into 5 rods (Rod 1, 3, 4, 5 and 10) at different positions, so a series of irradiation temperatures and doses was obtained. Table 1 gives the final irradiation temperature, doses and helium contents of the samples.

The SP test experimental configuration is shown schematically in Fig. 1. It consists of a clamped, centre-loaded disk specimen. The SP specimen holder consists of an upper and lower die, and four clamping screws. Using this specimen holder, the specimens are prevented from cupping upward during punching. Therefore plastic deformation is concentrated in the region below the punch (1 mm steel ball).

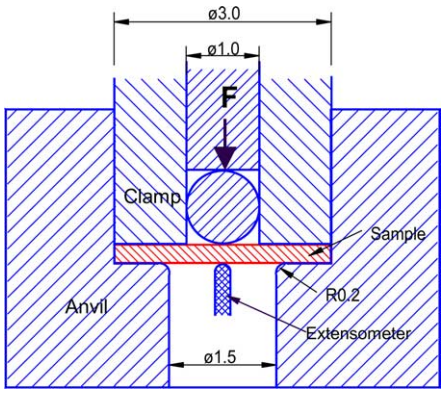

Fig. 1. A schematic diagram shows the set-up of small punch test.

The SP test was performed on a Zwick mechanical testing machine, with a maximum load capacity of 20 kN. A special low temperature device was designed to obtain testing temperatures from liquid nitrogen temperature to room temperature. For tests above room temperature, we use a small heat ring to heat the specimen from room temperature up to 300 °C together with the specimen die. The temperature was measured by a Type K NiCr-Ni (DIN IEC 584-1) thermocouple, placed into the specimen die 0.5 mm away from the specimen.

The testing was carried out at a constant crosshead speed of 0.1 mm min^{-1}. During testing, the load–displacement curve was measured both by the crosshead and an additional video-extensometer. All the testing data were automatically recorded. In order to get the ductile–brittle transition behaviour, about 15–20 unirradiated samples and about 6–8 irradiated samples were tested for each irradiation dose at different testing temperatures.

To understand the fracture mechanism, the fracture surfaces of SP samples for selected specimens were examined by scanning electron microscopy (SEM). For the unirradiated specimen, about eight samples from the whole testing temperature regime were observed. For irradiated ones, normally 3–5 samples were selected from lower to higher test temperature corresponding to the upper shelf energy, transition and lower shelf energy regimes to investigate the brittle-ductile transition behavior for each dose.

3. Results

SP test of unirradiated and irradiated F82H, T91 and Optimax-A steels were performed at temperatures from about −190 to 80 °C. Typical load–displacement curves

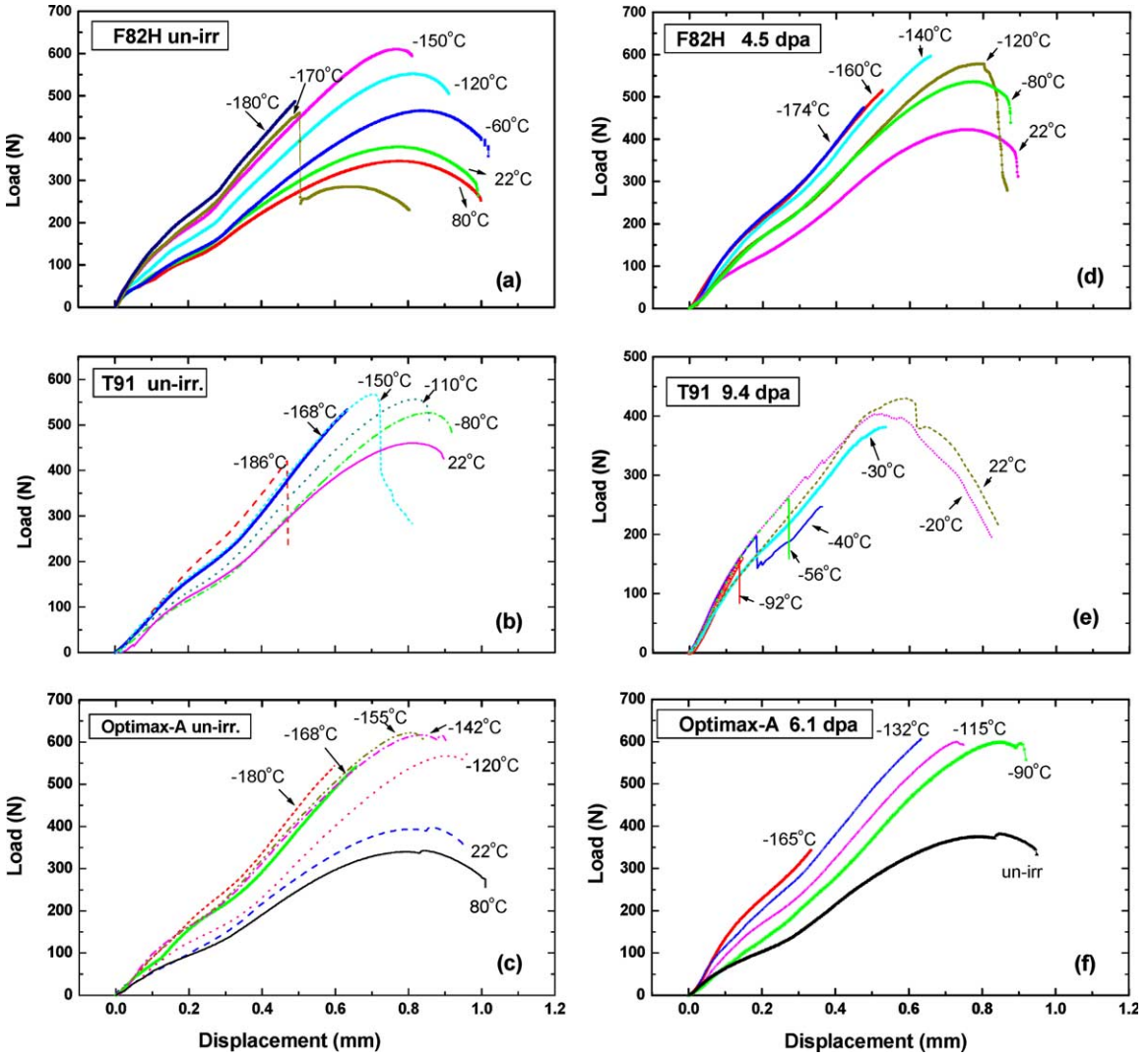

Fig. 2. Typical load–displacement curves for the three steels before and after irradiation: (a) F82H, un-irradiated; (b) T91, un-irradiated; (c) Optimax-A, un-irradiated; (d) F82H, 4.50 dpa, (e) T91, 9.35 dpa, and (f) Optimax-A, 6.10 dpa, respectively.

for these three materials before and after irradiation are presented in Fig. 2(a)–(f). As we can see, the SP yield load (P_y) and maximum load (P_{max}) increase generally with decreasing test temperature while the displacement at fracture (or the total displacement) decrease. For unirradiated samples tested at temperatures below about −160 °C, they break in the earlier stage of the curve before the maximum load is reached. This happens at higher temperatures for irradiated samples. There are actually no remarkable differences in the shape of the load–displacement curves for irradiated and unirradiated samples.

Fig. 3(a)–(c) illustrate the temperature dependence of SP fracture energy for F82H, T91 and Optimax-A steels at different irradiation doses. The $DBTT_{SP}$ is defined in a traditional way as the temperature corresponding to a SP fracture energy which is half the value of the upper shelf energy. The $DBTT_{SP}$ data are listed in Table 1. The uncertainty of the $DBTT_{SP}$ is less than ±10 °C. Fig. 4 presents the dose dependence of $\Delta DBTT_{SP}$ for the three steels. It shows that at lower irradiation doses, the $\Delta DBTT_{SP}$ increases linearly with the increasing of dose, but at irradiation dose higher than about 6–7 dpa with helium concentrations above about 400 appm, there is a substantial increase of $\Delta DBTT_{SP}$. The results show also that F82H has the lowest shift in $DBTT_{SP}$ as a function of dose among these three steels.

Fig. 5 shows the morphology of the SP samples of F82H steel tested at different temperatures before irradiation. The ductile–brittle fracture mode transition

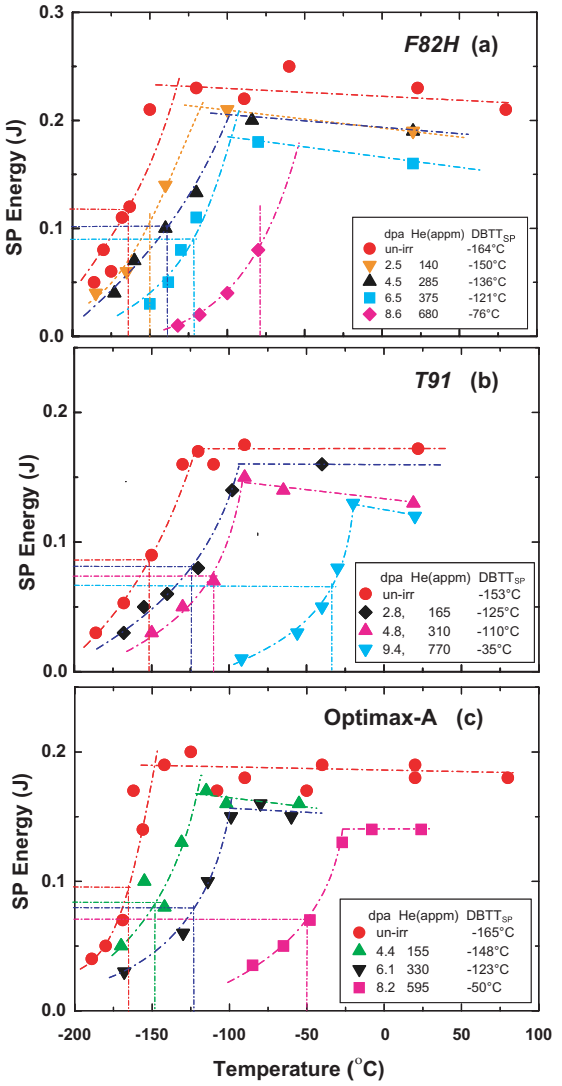

Fig. 3. The temperature dependence of SP fracture energy for F82H, T91 and Optimax-A steels at different irradiation doses, respectively.

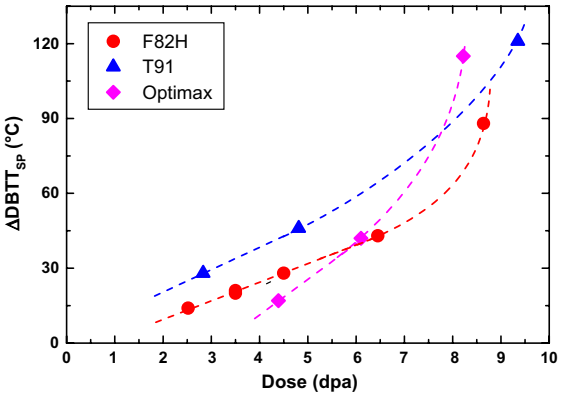

Fig. 4. The $\Delta DBTT_{SP}$ of the three steels as a function of irradiation dose.

behavior is clearly demonstrated. At lower temperatures, brittle cracks propagated along the radial direction (Fig. 5(g) and (h)). With increasing testing temperature, plastic bulging increased and ductile cracks propagated circumferentially in the heavily stretched part, which produced a large displacement of the specimen before cracking.

Fig. 6 presents the detail of the fracture surfaces for the corresponding samples shown in Fig. 5. As can be seen, the fracture was totally ductile at test temperatures down to −40 °C. Mixed ductile–brittle fracture appeared at test temperatures between −80 and −100 °C. The amount of brittle fracture increases with decreasing test temperature. At −160 °C, the fracture is completely brittle, and some inter-granular fracture feature was observed at −190 °C.

Fig. 7 gives the SEM micrographs for F82H samples after irradiation to 4.5 dpa. At room temperature, the specimen has a large deformation before fracture. The fracture is ductile. At −90 °C, the fracture is still ductile, but some brittle regions appear. The fracture becomes more brittle in character at −120 °C. At −150 °C, the fracture is completely cleavage fracture, and nearly no plastic deformation occurred before breaking. Few micro-cracks were observed on specimen surfaces at all the test temperatures, and no significant difference in the appearance of the micro-cracks was found between specimens tested at different temperatures.

Fig. 8 gives the SEM micrographs for T91 steel samples after irradiation to 9.4 dpa. At room temperature, the fracture is already a mix of ductile and cleavage fracture with about 30–40% cleavage. The amount of cleavage increases to about 60–70% at −20 °C and becomes almost 100% at −30 °C. At −90 °C, the main crack was initiated at the center of the specimen, and no plastic deformation occurred before the final fracture. The fracture was almost inter-granular.

4. Discussion

It is known that irradiation hardening is the main feature of metals irradiated in low temperature regime ($\leqslant 0.3\ T_m$, T_m is the absolute melting point temperature). The hardening is attributed to the irradiation induced defect structure. Our previous studies demonstrate that the microstructure of F82H and T91 has little temperature dependence when the irradiation temperature is below about 250 °C [10,11]. Above 250 °C, the density of defect clusters decreases while the size increases with irradiation temperature. In the present study, except two

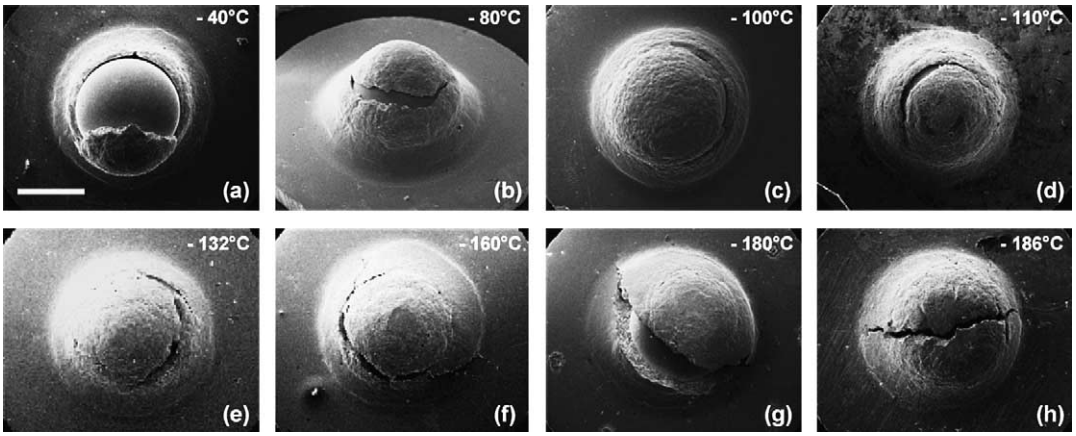

Fig. 5. SEM micrographs show the morphology of the un-irradiated F82H SP samples tested at different temperatures. The scale bar for all is shown in (a). It is 0.5 mm.

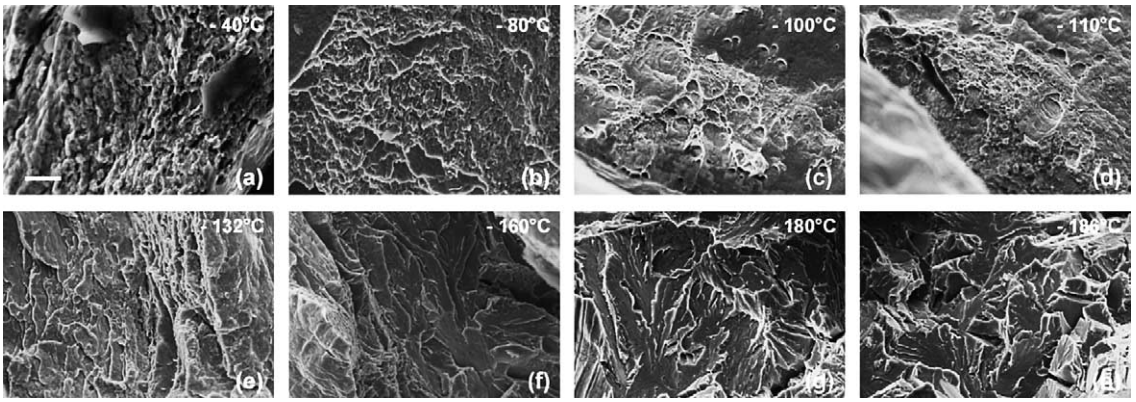

Fig. 6. SEM micrographs of a higher magnification show the fracture surfaces of the un-irradiated F82H SP samples presented in Fig. 5. The scale bar for all is shown in (a). It is 10 μm.

sets of samples were irradiated at 265 and 275 °C, all other samples were irradiated below 250 °C. Therefore, the irradiation temperature dependence of the present data is believed to be not significant.

To evaluate the yield strength (σ_y) of a material by means of small punch tests, Mao and Takahashi [12] have conducted both small punch tests and the standard tensile tests on a series of ferritic steels and acquired an empirical expression: $\sigma_y = 0.36P_y/t_0^2$, where P_y is the yield load in N and t is the initial specimen thickness in mm. In order to analyze whether the embrittlement is partially due to hardening, this empirical expression has been employed to estimate the yield strength of the material for each testing temperature. Fig. 9(a) and (b) represent the estimated yield strength as a function of test temperature for F82H and T91 steels before and after irradiation, respectively. In order to make a comparison, the yield strength data obtained from tensile tests for each material at unirradiated condition from Spaetig et al. [13] was also plotted. As can be seen, in case of F82H steel, the yield stresses estimated from the SP tests are about 100 MPa lower than the tensile data. With decreasing test temperature, the yield strength obtained either by SP or by tensile test increases, and this increase is more rapid at temperatures lower than about −100 °C. As it is well known, the yield stress of a material increases with decreasing temperature or increasing shear modulus. The rapid increase in yield stress with decreasing temperatures is normally associated with the Peierls' mechanism [14].

For T91 steel, the yield strength obtained by the SP tests is consistent with the data obtained by tensile tests. But the reference T91 steel was not the same materials as was studied in the SP tests. The material we used in the SP tests has nominal yield strength about 550 MPa at room temperature, but the yield strength of T91 steel

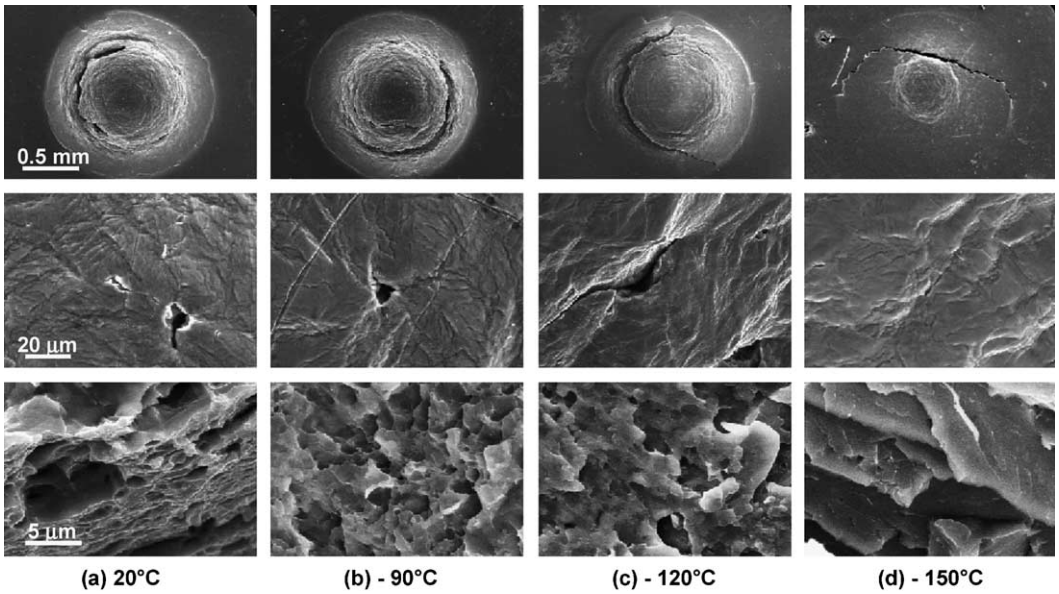

Fig. 7. SEM micrographs show F82H samples irradiated to 4.5 dpa tested at different temperatures. Three pictures (from up to down) of each column show the morphology, the micro-cracks on the surface and the fracture surface of the sample. The scales in the pictures of column (a) are the same for the corresponding pictures in other columns.

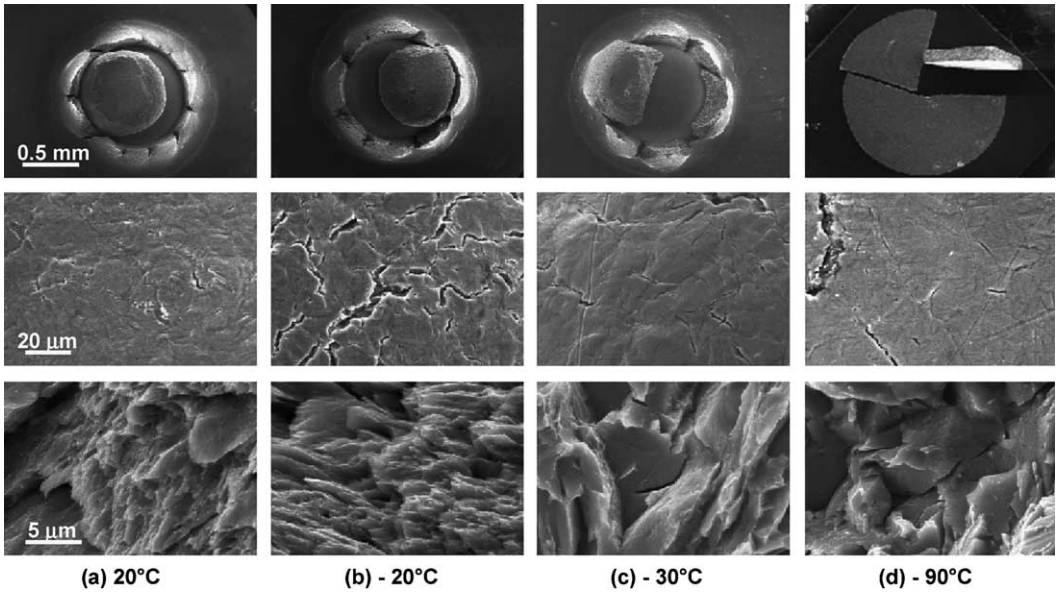

Fig. 8. SEM micrographs show T91 samples irradiated to 9.4 dpa tested at different temperatures. Three pictures (from up to down) of each column show the morphology, the micro-cracks on the surface and the fracture surface of the sample. The scales in the pictures of column (a) are the same for the corresponding pictures in other columns.

used by Spaetig et al. [13] for tensile tests had a yield strength of only 470 MPa at room temperature.

The reason why the SP values are about 100 MPa lower for both steels is not clear. It is probably due to the different installations and different materials. In the case of F82H steel, the expression is suggested to be $\sigma_y = 0.4P_y/t_0^2$. This expression might be applicable to the T91 steel, too.

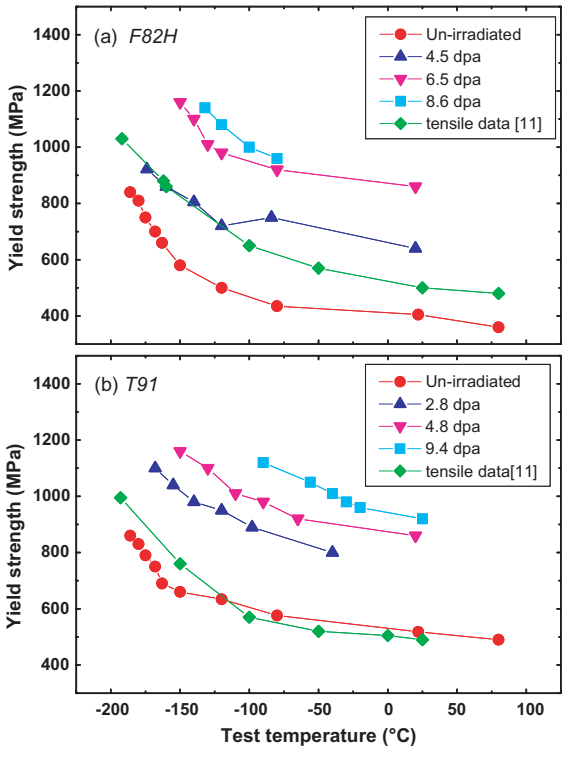

Fig. 9. The yield strength calculated using the expression $\sigma_y = 0.36P_y/t_0^2$ as a function of test temperature for the samples of F82H and T91 steels.

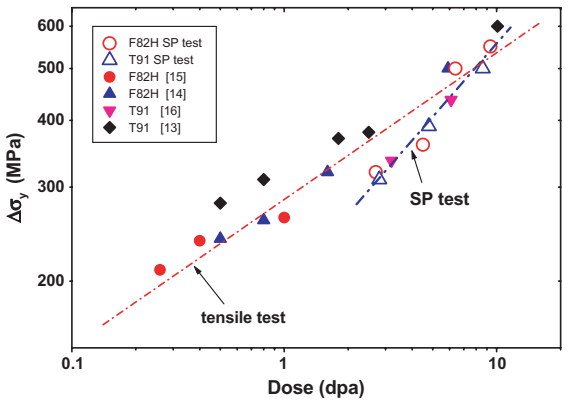

Fig. 10. A comparison of irradiation hardening in F82H and T91 steels by SP test and tensile test.

Using the expression $\sigma_y = 0.4P_y/t_0^2$, the irradiation hardening data from tests at room temperature is evaluated and plotted in Fig. 10. For comparison, the data from recent tensile tests on F82H and T91 irradiated with high-energy protons [15–18] at <300 °C were included. Results show that the irradiation hardening measured by the SP tests is consistent with the data from

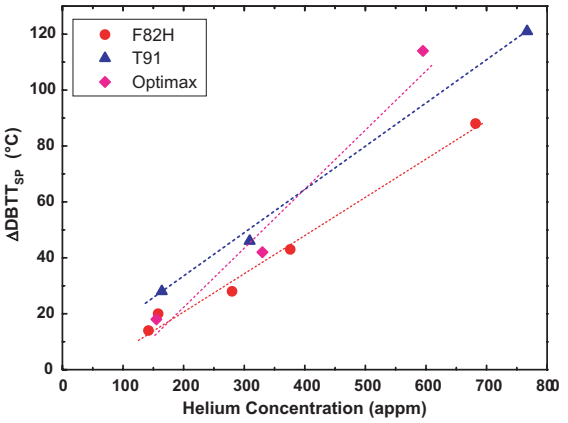

Fig. 11. The $DBTT_{SP}$ as a function of helium concentration

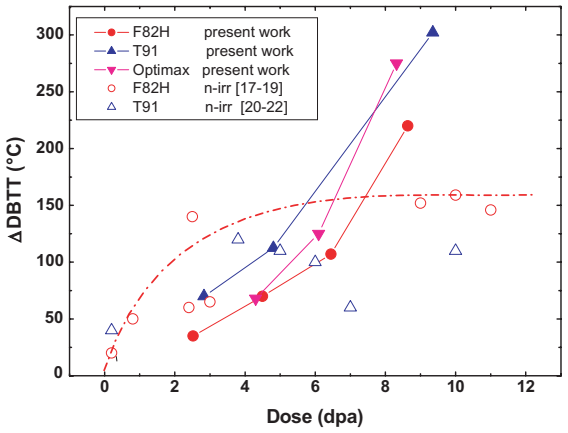

Fig. 12. A comparison of ΔDBTT for martensitic steels irradiated in fission reactors [17–22] and in SINQ Target-3.

tensile tests. A little higher slope for the SP data is found.

In the present irradiation, the ratio of He/dpa is not constant due to different proton and neutron spectra at different positions in the target [19]. This results in a different dependence of $\Delta DBTT_{SP}$ on helium concentration. Fig. 11 plots the $\Delta DBTT_{SP}$ as a function of helium concentration. It demonstrates that the $\Delta DBTT_{SP}$ increases linearly with helium concentration of the specimens. This increase in transition temperature is not reflected as comparable hardening due to the increasing helium content. Rather, the observed hardening is assigned to the defect cluster microstructure plus the presence of a high density of nano-voids (which produce additional hardening even without any helium being present).

Using the empirical expression $DBTT_{CVN} = 2.5\,DBTT_{SP}$ [10], comparable ΔDBTT can be obtained from the SP tests. Results are plotted in Fig. 12 together with

neutron-irradiation data [20–25]. They indicate very different trends for the two data sets. After neutron irradiation, the ΔDBTT increases with increasing irradiation dose and tends to saturate at a dose level of about 3–5 dpa (it should be pointed out that the neutron-irradiation values were obtained from sub-size either $3\times4\times27$ or $3.33\times3.33\times25.4$ mm^3 Charpy specimens, that show a lower DBTT than standard CVN specimens of, $10\times10\times55$ mm^3). However, the ΔDBTT does not saturate in the case of high-energy proton irradiation. In addition it increases more rapidly at the higher dose level of 6–7 dpa. The additional increase of $\Delta DBTT_{SP}$, may indicate that helium not only contributes to the hardening commensurate with the additional shift in the DBTT but also weakens the grain and lath boundaries to reduces the fracture stress.

5. Conclusion

The present results of martensitic/ferritic steels F82H, T91 and Optimax-A irradiated in SINQ Target-3 in a temperature range of 90–275 °C up to 9.4 dpa demonstrate that:

(a) The irradiation hardening deduced from SP tests is reasonably consistent with the results obtained by tensile tests.
(b) The $DBTT_{SP}$ increases with increasing irradiation dose, and more quickly at high irradiation doses above ~6–7 dpa. The $\Delta DBTT_{SP}$ increases linearly with the helium contents.
(c) Comparing to neutron irradiation, the irradiation in a proton-neutron mixed spectrum may introduce higher DBTT shift due to the high helium concentration at a high dose.

Acknowledgements

The authors would like to express thanks to Mr R. Thermer for his kindly help on SP tests, to Mr R. Bruetsch for his help on SEM observations, and to Drs M. Victoria and K. Farrell for supplying the steels and some useful discussions as well.

This work is included in both SPIRE (Irradiation effects in martensitic steels under neutron and proton mixed spectrum) subprogram of the European 5th Framework Program and ESS-TMR program, which are supported by Swiss Bundesamt feur Bildung und Wissenschaft.

References

[1] M. Tamura, H. Hayakasa, M. Tanimura, A. Hishinuma, T. Kondo, J. Nucl. Mater. 141–143 (1986) 1067.
[2] Y. Dai, ICANS-XII and 4th Plenary Meeting of the ESS Project (ESS-PM4), 1995.
[3] F.M. Huang, M.L. Hamilton, G.L. Wire, Nucl. Technol. 57 (1982) 234.
[4] M.P. Manahan, Nucl. Technol. 63 (1983) 275.
[5] J.M. Baik, J. Kameda, O. Buck, Scr. Metall. 17 (1983) 1443.
[6] K. Farrell, private communication.
[7] Y. Kohno, D.S. Gelles, A. Kohyama, M. Tamura, A. Hishinuma, J. Nucl. Mater. 191–194 (1992) 868.
[8] M. Victoria, CRPP/EPFL report.
[9] Y. Dai, G.S. Bauer, J. Nucl. Mater. 296 (2001) 43.
[10] X. Mao, H. Takahashi, J. Mater. Sci. 27 (1992) 983.
[11] X. Jia, Y. Dai, M. Victoria, J. Nucl. Mater. 305 (2002) 1.
[12] X. Jia, Y. Dai, J. Nucl. Mater. 318 (2003) 207.
[13] P. Spaetig, G.R. Odette, G.E. Lucas, J. Nucl. Mater. 275 (1999) 324.
[14] R. Peierls, Proc. Phys. Soc. 52 (1940) 34.
[15] K. Farrell, T.S. Byun, J. Nucl. Mater. 296 (2001) 129.
[16] Y. Dai, S.A. Maloy, G.S. Bauer, W.F. Sommer, J. Nucl. Mater. 283–287 (2000) 513.
[17] P. Spaetig et al., J. Nucl. Mater. 258–263 (1998) 1345.
[18] Y. Dai, X. Jia, K. Farrell, J. Nucl. Mater. 318 (2003) 192.
[19] Y. Dai, Y. Foucher, M.R. James, B.M. Oliver, J. Nucl. Mater. 318 (2003) 167.
[20] E.V. van Osch, in: R.L. Klueh (Ed.), Proceeding of the IEA workshop/working group meeting on Ferritic/Martensitic steels, Petten, Netherlands, 1998.
[21] M. Rieth, B. Dafferner, H.D. Roehrig, J. Nucl. Mater. 258–263 (1998) 1147.
[22] R.L. Klueh, M.A. Sokolov, K. Shiba, J. Nucl. Mater. 283–287 (2000) 478.
[23] R. Klueh, D.J. Alexander, 18th Int. Symp., ASTP STP 1325 (1999) 911.
[24] R. Klueh, D.J. Alexander, J. Nucl. Mater. 187 (1992) 60.
[25] J.J. Kai, R. Klueh, J. Nucl. Mater. 230 (1996) 116.